

## Geochemical Characterization of a Fibrous Calcite Vein Using Micro X-ray Fluorescence Imaging: A Case Study

Tindikorn Kanta <sup>1,\*</sup>

<sup>1</sup> Department of Geology, Faculty of Science, Chulalongkorn University, Thailand

\* Corresponding author: tindikorn@gmail.com

Received: 07 May 2025

Revised: 30 Jun 2025

Accepted: 03 Jul 2025

### Abstract

Micro-X-ray fluorescence ( $\mu$ XRF) imaging is an effective non-destructive method extensively utilized in geosciences for the acquisition of high-resolution spatial elemental data. This study utilizes  $\mu$ XRF coupled with the petrographic observations and conventional geochemical analyses (XRF, XRD, and ICP-MS) to examine a fibrous calcite vein (KK1) from the Permian Khao Khwang Formation in Thailand. The calcite vein, devoid of attached host rock, displays a cone-in-cone texture and a median suture rich in inclusions.  $\mu$ XRF elemental maps indicate a Ca-dominant composition, with median enrichments observed in Fe, Si, Al, K, and Mn, suggesting the presence of clay-rich inclusions. Additionally, trace element zonation patterns—particularly Mn and Sr—indicate evolving redox conditions and fluid composition during vein growth. The Mn-enriched median region suggests early precipitation under reducing, possibly organic-rich pore waters, followed by calcite crystallization under progressively more oxidizing conditions. Sr mapping highlights later-stage, Sr-rich cross-cutting veinlets, pointing to multiple fluid episodes. These findings support a model of progressive burial diagenesis and fluid-mediated vein formation. Overall, this study illustrates the capability of  $\mu$ XRF to improve comprehension of fluid history, mineral development, and redox conditions within sedimentary systems, thereby assisting geologists in basin analysis and petroleum system assessment.

**Keywords:** Khao Khwang Formation, trace elements, diagenesis, carbonate rock

## 1. Introduction

Micro-X-ray fluorescence ( $\mu$ XRF) is a powerful analytical technique increasingly used in geosciences for high-resolution elemental analysis. It enables non-destructive elemental mapping of samples at the microscale, making it invaluable in a variety of fields including geology, mineralogy, and paleontology (Kaskes et al., 2021). In geological research,  $\mu$ XRF has been applied to analyze rocks and minerals, perform material characterization, and map elemental distributions in sedimentary and igneous contexts (Fabre et al., 2022; Gabriel et al., 2022; Genna et al., 2011; Nikonow et al., 2019; Potter & and Brand, 2019). The ability of  $\mu$ XRF to rapidly produce two-dimensional elemental distribution maps is especially useful for visualizing geochemical zonation and inclusions within minerals and rocks. For example,  $\mu$ XRF mapping can identify mineral phases based on their elemental signatures and reveal subtle compositional banding or zoning that would be difficult to detect with bulk analyses (Trebis et al., 2022). In mineralogical studies, this technique helps correlate elemental variations with mineral textures, aiding in phase identification and understanding crystal growth histories (Sirbescu et al., 2023). All are achieved non-invasively and with minimal sample preparation.

Given its broad utility,  $\mu$ XRF is an ideal tool for investigating the spatial geochemistry of complex geological samples such as bedding-parallel fibrous calcite veins. These fibrous calcite veins (often called "beef" or cone-in-cone structures in the literature) are widespread in sedimentary basins and are particularly associated with organic-rich sequences (e.g. petroleum source rocks) (Al-Aasm et al., 1995;

Luan et al., 2019; Sun et al., 2023). However, their formation processes remain debated, in part due to limited high-resolution geochemical data. This study used  $\mu$ XRF imaging on a representative fibrous calcite vein from the Permian Khao Khwang Formation in central Thailand to delineate the elemental distribution and microstructural characteristics inside the vein. The objective is to obtain a comprehensive understanding of the vein's internal zonation and composition by combining  $\mu$ XRF elemental maps with traditional geochemical assays and petrographic observations. This method enables the identification of elemental enrichments or depletions in particular sections of the vein (including median zones, inclusion-rich bands, or subsequent cross-cutting veinlets), thereby offering insights into the vein's growth mechanism and the chemical evolution of the precipitating fluids.

This study highlights the potential of  $\mu$ XRF to visualize geochemical zonation in vein samples, which can inform future research on similar geological issues. Geologists can better understand rock diagenetic processes by linking geochemical anomalies with textural features using  $\mu$ XRF maps.

In summary, this study not only sheds light on the formation of an unusual fibrous calcite vein in the Khao Khwang Formation, but also showcases the utility of  $\mu$ XRF as a modern tool for spatial geochemical analysis in geoscience research. This information can ultimately help in reconstructing fluid histories in basins and may have practical implications, for example, in understanding indicators of hydrocarbon maturation and migration in the region.

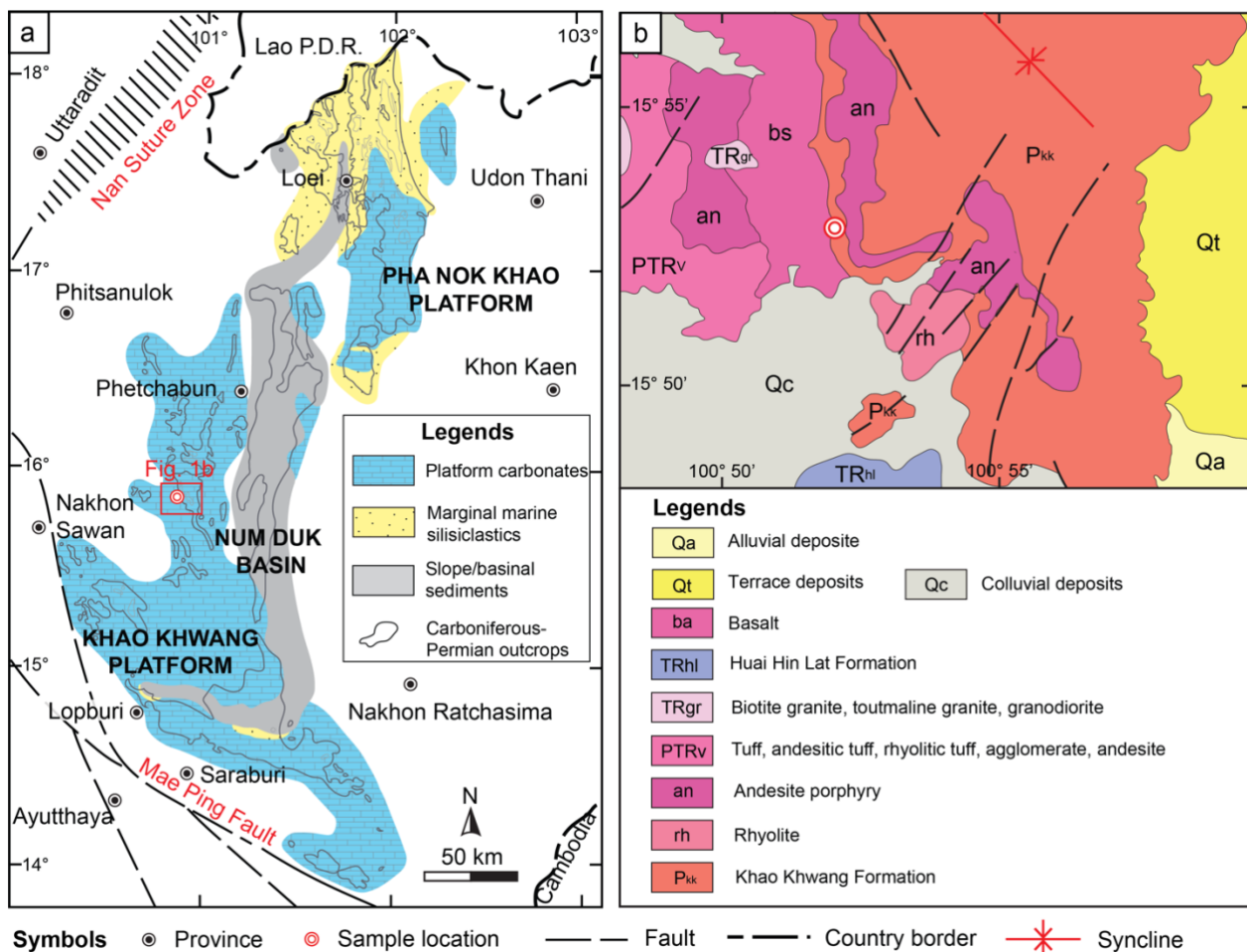


**Figure 1.** Location map of the study area showing (a) the distribution of the Permian major facies subdivisions on the western margin of the Indochina Block (Ueno & Charoentitirat, 2011) , and geological map of the study area.

## 2. Material and Method

### 2.1. Sample and preparation

The fibrous calcite vein sample (labelled KK1) was collected from the Permian Khao Khwang Formation, where it occurs as a bedding-parallel vein within carbonate host rocks (Figure 2). The KK1 sample is a single vein specimen (~4.5 cm thick) with a well-developed fibrous texture and a median inclusion-rich zone. A petrographic thin section of KK1 was prepared to expose a cross-section of the vein for microscopic and  $\mu$ XRF analysis. Standard thin sections (30  $\mu$ m thickness) were

used for elemental mapping to ensure a flat, smooth surface and representative cross-sectional view of the vein's internal features. Prior to  $\mu$ XRF analysis, the thin section and polished slab were thoroughly cleaned and dried, but no chemical treatment or coating was applied.

A thin section of KK1 was analyzed by  $\mu$ XRF to map element distributions. The section was scanned under vacuum with a 25  $\mu$ m step size, collecting fluorescence spectra at each point. Elemental intensity maps for Ca, Fe, Mg, Mn, Si, Al, K, Sr, and S were obtained by

integrating the characteristic X-rays of each element.

Bulk geochemical analyses were performed to quantify the vein's composition. A portion of the KK1 vein was powdered for analysis. Major elements were measured using XRF on a pressed pellet with the Bruker model S4 Pioneer WDXRF machine, while trace elements (including REEs) were measured using ICP-MS on dissolved sample solutions with the Analytik Jena PlasmaQuant MS Elite. Standard calibration procedures were followed. Moreover, the mineral composition of the sample was analyzed by XRD conducted using the XRD instrument Model D8 Advance, Bruker AXS, 40 kV, and 30 mA. All procedures were conducted at the Department of Geology, Faculty of Science, Chulalongkorn University.

## 2.2. $\mu$ XRF analysis

Elemental mapping of the KK1 calcite vein was conducted using a benchtop micro-X-ray fluorescence spectrometer (Bruker M4 Tornado) equipped with an XFlash® 430 silicon drift detector at the Department of Geology, Faculty of Science, Chulalongkorn University. The instrument operated at 50 kV and 600  $\mu$ A under low vacuum conditions (1.9 mbar) to improve sensitivity to light elements. Samples were raster-scanned with a pixel size of  $\sim$ 100  $\mu$ m for slab specimens and 200  $\mu$ m for thin sections, covering the entire vein cross-section. Data were acquired and processed using the Bruker M4 Tornado software. Elemental maps were generated for Ca, Fe, Mg, Si, Al, K, Mn, S, and Sr based on their characteristic fluorescence peaks. Peak overlaps were resolved and background noise removed to produce qualitative intensity maps. These maps were not normalized to absolute concentrations; rather,

color intensity indicates relative elemental distribution. Final maps were analyzed alongside optical images to correlate geochemical features with petrographic observations such as inclusion bands, crystal terminations, and micro-veinlets.

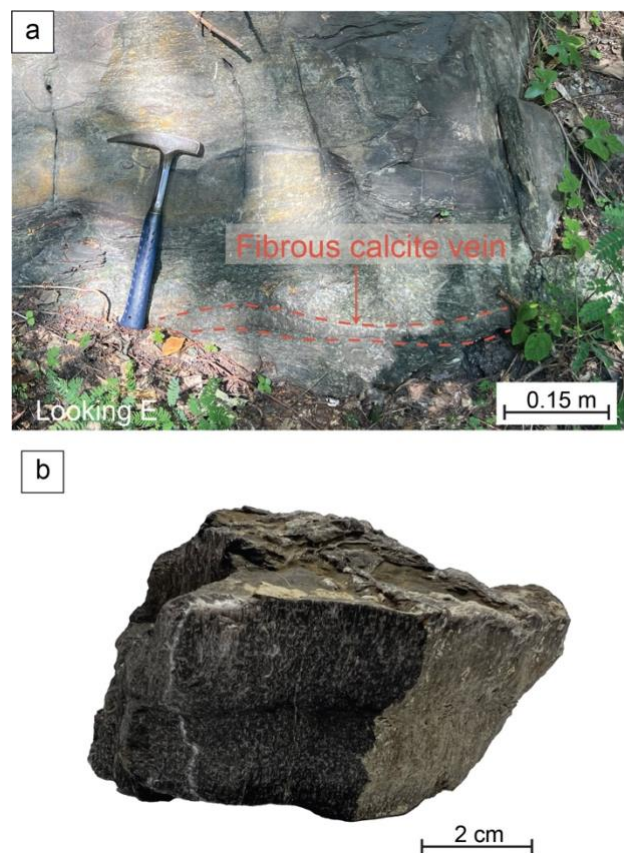


**Figure 2.** (a) The bedding-parallel fibrous calcite vein in the outcrop. (b) Hand specimen of the KK1 sample.

## 2.3. Interpretation approach

The  $\mu$ XRF elemental maps were interpreted by identifying spatial variations in element distribution and correlating them with vein microstructures. Elemental enrichments and depletions were cross-validated with bulk geochemical data obtained from XRF (major elements), ICP-MS (trace elements), and XRD (mineralogical composition). While bulk

analyses provided quantitative values,  $\mu$ XRF offered spatial context within the vein. This integrated approach enabled the verification of elemental trends and distribution. The interpretation focuses on the fibrous vein, with host rock data included only when relevant to vein characterization.

### 3. Results and interpretations

#### 3.1. Petrography of KK1 Vein

In thin section, the KK1 fibrous calcite vein shows a classic internal zoning (Figure 3). The median line is a narrow band containing layered, brownish opaque inclusions parallel to the vein. On either side, fibrous calcite crystals radiate outward toward the vein walls (Figure 3a, c, e). The fibrous calcite exhibits a cone-in-cone structure: fibrous bundles are separated by curved inclusion-rich seams that trace conical shapes rooted at the median (Figure 3b). The outer parts of the vein consist of clearer calcite with fewer inclusions, terminating sharply against the former host rock interface. The median inclusion band divides the vein into two symmetrical halves, consistent with antitaxial (center-growing) vein formation. Locally, small veinlets of sparry calcite cross-cut the fibrous texture at high angles; these veinlets are inclusion-poor and represent later crack-seal events that post-date the main fibrous vein (Figure 3f).

#### 3.2. Bulk Composition of the Fibrous Calcite Vein

##### 3.2.1. Major elements and minerals

Geochemical analysis confirms that the KK1 fibrous vein is composed predominantly of calcite ( $\text{CaCO}_3$ ), with minor silicate and oxide impurities as identified by XRD analysis. The bulk major oxide composition of the vein shows

49.5 wt.%  $\text{CaO}$ , corresponding to calcite as the major mineral (Table 1). Loss on ignition (40.5 wt.%) accounts for the  $\text{CO}_2$  in calcite, consistent with a nearly pure carbonate. Minor constituents include  $\text{SiO}_2$  (5.2 wt.%),  $\text{Al}_2\text{O}_3$  (1.7 wt.%),  $\text{MgO}$  (0.8 wt.%), and  $\text{Fe}_2\text{O}_3$  (0.6 wt.%), indicating a small fraction of clay or shale material mixed into the vein, likely as microscopic inclusions. Notably,  $\text{MnO}$  is present at about 0.26 wt.%. The KK1 vein's host rock (not present in this particular sample) is a carbonate shale, so it is likely that some detrital or organic material from the host was incorporated into the vein during its growth, explaining the small amounts of Si, Al, K, Fe, and Mn in the bulk chemistry.

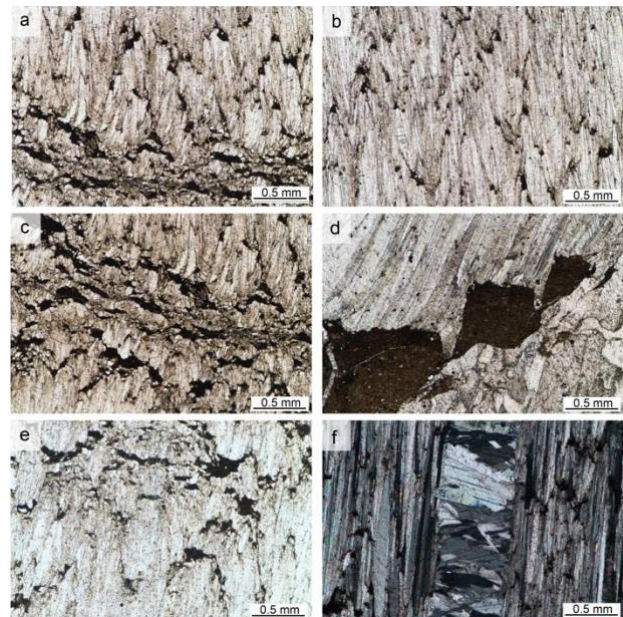


**Figure 3.** Photomicrographs of the KK1 sample. (a) The median suture line and cone-in-cone structure; (b) Cone-in-cone structure in the upper part of the suture line; (c) The median suture line; (d) The solid inclusion in the fibrous calcite vein; (e) Cone-in-cone structure in the lower part of the suture line; (f) Smaller vein in the fibrous calcite vein.

Table 1 presents detailed mineral compositions obtained from XRD analysis of the samples. The fibrous calcite veins are notably rich in calcite and contain only minor amounts of quartz, reflecting a carbonate-dominated lithotype.

**Table 1.** Semi-quantitative XRD results showing the mineral composition of the fibrous calcite vein sample (KK1).

Sample	Mineral Composition Content (wt.%)		
	Calcite	Quartz	Total
KK1	98.97	1.03	100

### 3.2.2. Trace elements

ICP-MS trace element analysis of the vein (Table 2) shows Sr around 4,743 ppm and Se around 1,709 ppm, making these two elements the most abundant trace constituents of KK1. The fibrous calcite vein is strongly enriched in strontium (Sr) and selenium (Se) compared to typical sedimentary calcites. Other trace metals are found at significantly lower concentrations: for instance, barium (Ba) is typically in the range of a few tens of ppm, lead (Pb) measures 27 ppm, while transition metals such as V, Cr, Ni, Cu, and Zn vary from tens to a few hundred ppm. The presence of manganese (Mn) in the vein is noteworthy, indicating concentrations of several thousand ppm of Mn.

**Table 2.** Geochemical composition of calcite vein using XRF and ICP-MS analyses.

Sample	CaO	SiO <sub>2</sub>	Al <sub>2</sub> O <sub>3</sub>	Fe <sub>2</sub> O <sub>3</sub>	MgO	K <sub>2</sub> O	MnO	Na <sub>2</sub> O	TiO <sub>2</sub>	P <sub>2</sub> O <sub>5</sub>	LOI	Total
	49.51	5.17	1.74	0.56	0.81	0.32	0.26	0.07	0.07	0.04	40.54	99.09
KK1	Se	Sr	Cs	Pb	As	V	Cr	Co	Ni	Cu	Zn	(ppm)
	1709.4	4742.7	<DL	27.1	<DL	159.2	211.1	94.6	164.1	362.1	349.9	

Note: DL= lower detection limit

**Table 3.** Elemental composition of fibrous calcite vein (KK1) in thin section and polished slab using  $\mu$ XRF analysis.

Elements (wt.%)	CaO	SiO <sub>2</sub>	Al <sub>2</sub> O <sub>3</sub>	Fe <sub>2</sub> O <sub>3</sub>	MnO	MgO	K <sub>2</sub> O	TiO	SrO	SO <sub>3</sub>	ZrO <sub>2</sub>	total
Thin section	80.41	9.99	3.92	3.07	0.91	0.70	0.26	0.34	0.18	0.20	0.02	100
Polished slab	81.27	9.02	3.14	3.01	1.15	0.62	0.21	0.27	0.11	1.16	0.04	100

### 3.3 Elemental Distribution from $\mu$ XRF Mapping

The  $\mu$ XRF elemental maps of the KK1 vein (Figures 4 and 5) illustrate the internal geochemical zonation of a fibrous calcite vein, which was initially noted in thin section and is now further clarified through the analysis of a polished slab. The thin section data reveal a central dark median line flanked by expansive, light-colored calcite zones, while elemental maps highlight an obvious Ca signal across the sample, affirming the predominance of calcite (Figures 4 and 5). The median suture exhibits a slight decrease in Ca intensity, which aligns with the inclusion-rich central seam, whereas minor Ca variations indicate localized inclusions and features from the late stage (Figure 5). Silicon, aluminum, and potassium exhibit significant concentration along the median line and in specific inclusion areas (Figures 4 and 5), probably indicating the presence of clay or mica phases that were introduced during the process of vein formation. The presence of these elements, almost absent in the cleaner calcite domains, highlights the integration of host-rock residues along the central vein axis. The co-enrichment of Fe and Mg in these zones indicates the presence of Fe-Mg-bearing clays or mixed carbonates (Figures 4 and 5). The data indicates a clear trend for Mn, characterized by enrichment close to the median and a decline as one moves outward (Figures 4 and 5). This observation implies a zoned incorporation of Mn into the early-formed calcite under reducing conditions. In contrast, Sr

exhibits a heterogeneous distribution, with the highest intensities observed in younger cross-cutting fibrous veinlets, suggesting late fluid influxes (Figures 4 and 5).

Recent observations from the polished slab (Figure 5) offer a more comprehensive perspective of the entire vein, uncovering further structural and chemical characteristics that were not entirely apparent in the thin section. The outer margins of the calcite vein exhibit an abundance of solid inclusions that are systematically aligned parallel to the central median line (Figure 5). The inclusions exhibit greater concentrations of Fe, Mg, Si, Al, K, and Sr, while demonstrating a significant reduction in Mn levels (Figure 5). This elemental signature supports the notion that these outer inclusions consist of clay-rich or altered host rock material that was incorporated during the process of vein growth. The correlation of these inclusions with the median indicates that they could represent initial growth fabrics or fluid pathways that remained consistent during the evolution of the vein. Their consistent orientation and composition offer additional support for a sustained antitaxial growth mechanism that integrated non-carbonate material from the surrounding rock into the developing vein system. The reduction of Mn in these inclusions, in contrast to its accumulation near the central median, highlights a geochemical difference between core and margin materials, probably influenced by fluid chemistry or redox gradients throughout vein development.

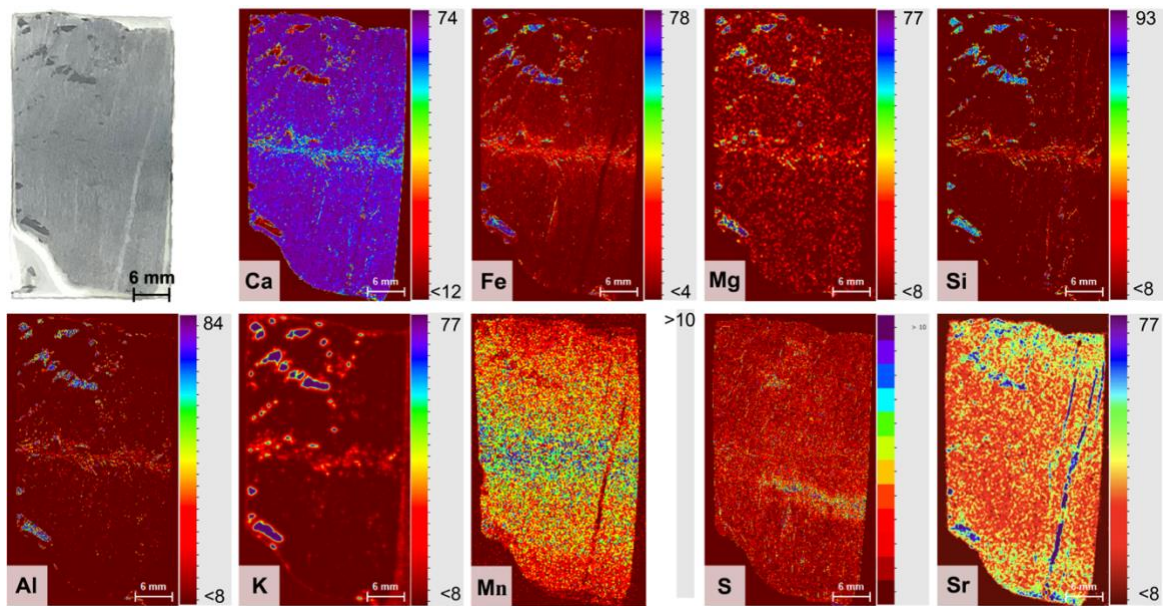


**Figure 4.** Element distribution of the bedding-parallel fibrous calcite vein in the thin section of the KK1 sample. The top-left image presents a scan of the sample, while each subsequent image represents the intensity of a specific element.

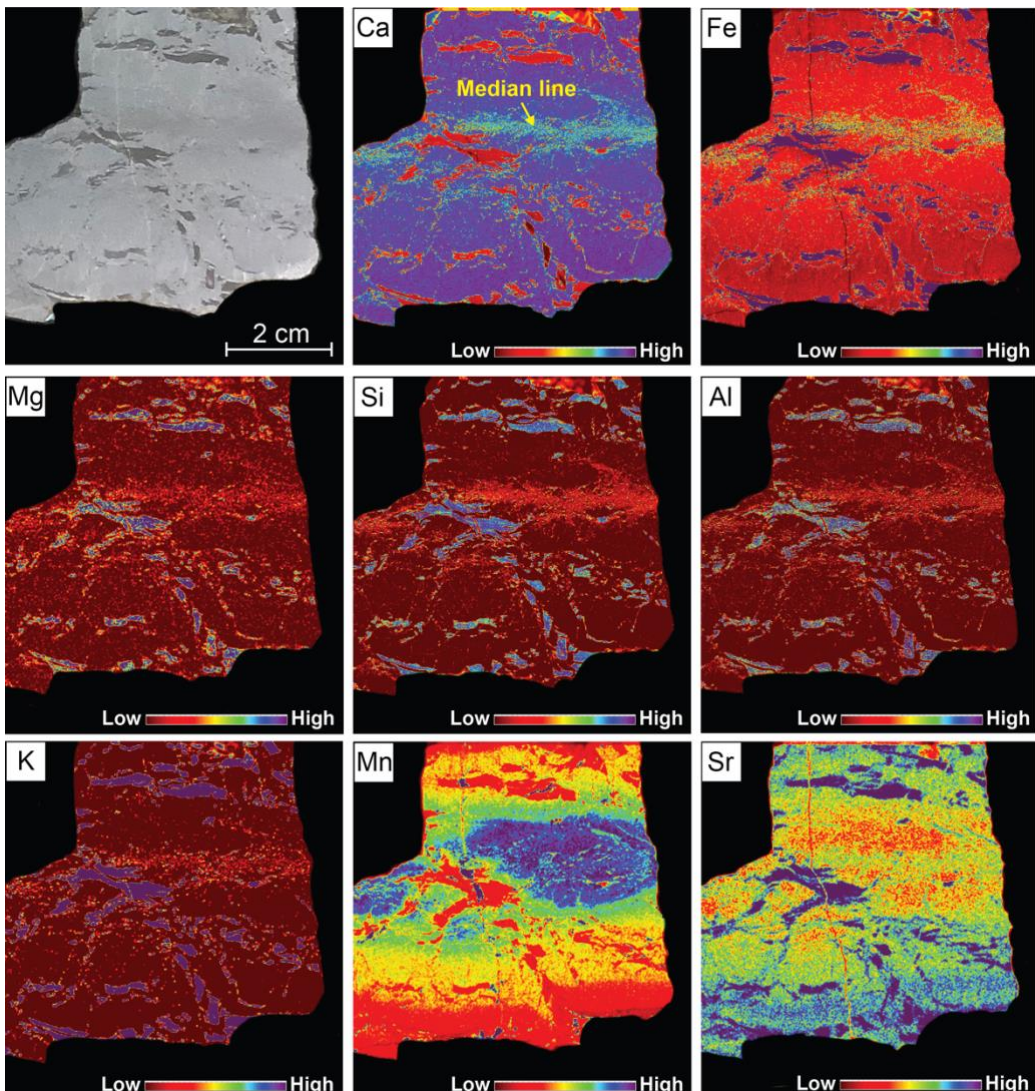


**Figure 5.** Element distribution of the bedding-parallel fibrous calcite vein in the polished slab of the KK1 sample. The top-left image presents a scan of the sample, while each subsequent image represents the intensity of a specific element.

#### 4. Discussions

##### 4.1 Formation of Fibrous Calcite Veins

Progressive burial diagenesis, characterized by mineral formation influenced by continuous fracturing and fluid migration under pressure, results in the development of fibrous calcite veins, commonly referred to as "beef" or cone-in-cone structures (Cobbold et

al., 2013; Meng et al., 2019). The geochemical characteristics of the KK1 fibrous calcite vein in the Permian Khao Khwang Formation indicate its formation conditions. Higher concentrations of strontium (Sr) and selenium (Se) indicate that vein-forming fluids interacted with marine carbonate or organic-rich host rocks,

precipitating from connate water and organically influenced fluids in reducing conditions (Mucci, 2004; Ngia et al., 2019). This study also emphasizes the distribution of trace elements, including Mn and Sr, within the vein, as revealed by  $\mu$ XRF analysis. These elements function as tracers for redox conditions and fluid sources (Elbaz-Poulichet et al., 2005). The observed Mn zonation, characterized by enrichment in the vein core and depletion outward, as depicted in Figures 4 and 5, indicates a shift in redox state or chemical conditions during calcite growth. It is likely that the earliest precipitated calcite, located at the median, formed under more reducing conditions that facilitated  $Mn^{2+}$  uptake, while subsequent calcite experienced either more oxidizing conditions or Mn-depleted fluids. This interpretation supports the hypothesis that fibrous calcite veins develop during progressive burial diagenesis, beginning with initial growth in anoxic, organic-rich pore waters (thus incorporating Mn and possibly Se), and subsequently continuing as conditions change.

#### 4.2 Application of $\mu$ XRF in Geochemical Zonation and Mineral Distribution

The  $\mu$ XRF mapping employed in this study facilitated the visualization of geochemical zonation, thereby enhancing our comprehension of the chemical variability and mineralogical domains of the KK1 vein. Conventional bulk chemical analysis and localized point measurements fail to adequately represent spatial elemental distributions. XRF analysis identified a median zone characterized by elevated concentrations of Fe, Al, Si, K, and Mg, suggesting the presence of clay-rich inclusions likely derived from the host rock. The distinct distribution of Mn and Sr observed in

$\mu$ XRF points out its utility. Mn mapping demonstrated minor yet significant fluctuations, highlighting areas of high concentrations near the median region of the vein, which suggests variations in fluid chemistry or redox conditions during its formation. Sr mapping identified strontium-enriched later-stage cross-cutting veinlets, suggesting successive fluid events and stages of mineral precipitation that were missed in petrographic observations. The  $\mu$ XRF method enables non-destructive analysis of samples, requires minimal preparation, and facilitates rapid data acquisition for thin sections. The rapid scanning and meso-scale elemental maps can inform more detailed analytical techniques that can help to clarify the result, including electron microprobe or laser ablation inductively coupled plasma mass spectrometry (LA-ICP-MS) (Alfeld and Janssens, 2015). The ability of XRF to spatially resolve elemental distributions is essential for geologists investigating the fluid history of sedimentary basins, diagenetic processes, and mineralization sequences. The integration of  $\mu$ XRF with conventional geological tools improves our comprehension of geological processes.

#### 5. Conclusion

Micro-XRF imaging of the KK1 fibrous calcite vein from the Permian Khao Khwang Formation reveals detailed geochemical zoning within the vein structure. The technique identified a Ca-rich calcite matrix with Fe, Mg, Mn, and clay-rich median zones, along with Sr-rich cross-cutting features. These patterns provide insight into vein formation mechanisms, including antitaxial growth, local fluid derivation, and post-veinlet cementation events. The integration of  $\mu$ XRF imaging with

petrographic and chemical analysis offers a powerful, non-destructive approach to interpreting fluid-rock interactions in sedimentary basins, with applications in petroleum geology and diagenesis research globally.

**Acknowledgments:** I would like to thank the Department of Geology, Faculty of Science, Chulalongkorn University, for access to laboratory facilities and analytical instruments. I also acknowledge the support of the micro-XRF imaging facility team and reviewers whose comments greatly improved the quality of this manuscript.

## References

Al-Aasm, I. S., Coniglio, M., & Desrochers, A., 1995. Formation of complex fibrous calcite veins in Upper Triassic strata of Wrangellia Terrain, British Columbia, Canada. *Sedimentary Geology*, 100(1), 83-95.

Alfeld, M., & Janssens, K., 2015. Strategies for processing mega-pixel X-ray fluorescence hyperspectral data: A case study on a version of Caravaggio's painting Supper at Emmaus. *Journal of Analytical Atomic Spectrometry*, 30.

Cobbold, P. R., Zanella, A., Rodrigues, N., & Loseth, H., 2013. Bedding-parallel fibrous veins (beef and cone-in-cone): Worldwide occurrence and possible significance in terms of fluid overpressure, hydrocarbon generation and mineralization. *Marine and Petroleum Geology*, 43, 1-20.

Elbaz-Poulichet, F., Seidel, J., Jézéquel, D., Metzger, E., Prevot, F., Simonucci, C., Sarazin, G., Viollier, E., Etcheber, H., Jouanneau, J.-M., Weber, O., & Radakovitch, O., 2005. Sedimentary record of redox-sensitive elements (U, Mn, Mo) in a transitory anoxic basin (the Thau lagoon, France). *Marine Chemistry*, 95, 271-281.

Fabre, C., Trebus, K., Tarantola, A., Cauzid, J., Motto-Ros, V., & Voudouris, P., 2022. Advances on microLIBS and microXRF mineralogical and elemental quantitative imaging. *Spectrochimica Acta Part B: Atomic Spectroscopy*, 194, 106470.

Gabriel, J. J., Reinhardt, E. G., Chang, X., & Bhattacharya, J. P., 2022. Application of  $\mu$ XRF analysis on the Upper Cretaceous Mancos Shale: A comparison with ICP-OES/MS. *Marine and Petroleum Geology*, 140, 105662.

Genna, D., Gaboury, D., Moore, L., & Mueller, W. U., 2011. Use of micro-XRF chemical analysis for mapping volcanogenic massive sulfide related hydrothermal alteration: Application to the subaqueous felsic dome-flow complex of the Cap d'Ours section, Glenwood rhyolite, Rouyn-Noranda, Québec, Canada. *Journal of Geochemical Exploration*, 108(2), 131-142.

Kaskes, P., Déhais, T., Graaff, S., Goderis, S., & Claeys, P., 2021. Micro-X-ray fluorescence ( $\mu$ XRF) analysis of proximal impactites: High-resolution element mapping, digital image analysis, and quantifications. In.

Luan, G., Dong, C., Azmy, K., Lin, C., Ma, C., Ren, L., & Zhu, Z., 2019. Origin of bedding-parallel fibrous calcite veins in lacustrine black shale: A case study from Dongying Depression, Bohai Bay Basin. *Marine and Petroleum Geology*, 102, 873-885.

Meng, Q., Hooker, J., & Cartwright, J. O. E., 2019. Role of pressure solution in the formation of bedding-parallel calcite veins in an immature shale (Cretaceous, southern UK). *Geological Magazine*, 156(5), 918-934.

Mucci, A., 2004. The Behavior of Mixed Ca-Mn Carbonates in Water and Seawater: Controls of Manganese Concentrations in Marine Porewaters. *Aquatic Geochemistry*, 10, 139-169.

Ngia, N. R., Hu, M., Gao, D., Hu, Z., & Sun, C.-Y., 2019. Application of Stable Strontium Isotope Geochemistry and Fluid Inclusion Microthermometry to Studies of Dolomitization of the Deeply Buried Cambrian Carbonate Successions in West-Central Tarim Basin, NW China. *Journal of Earth Science*, 30, 176-193.

Nikonow, W., Rammlmair, D., Meima, J. A., & Schodlok, M. C., 2019. Advanced mineral characterization and petrographic analysis by  $\mu$ -EDXRF, LIBS, HSI and hyperspectral data

merging. *Mineralogy and Petrology*, 113(3), 417-431.

Potter, N., & and Brand, N., 2019. Application of micro-XRF to characterise diamond drill-core from lithium-caesium-tantalum pegmatites. *ASEG Extended Abstracts*, 2019(1), 1-4.

Sirbescu, M.-L. C., Doran, K., Konieczka, V. A., Brennan, C. J., Kelly, N. M., Hill, T., Knapp, J., & Student, J. J., 2023. Trace element geochemistry of spodumene megacrystals: A combined portable-XRF and micro-XRF study. *Chemical Geology*, 621, 121371.

Sun, N., He, W., Zhong, J., Gao, J., Chen, T., & Swennen, R., 2023. Widespread development of bedding-parallel calcite veins in medium–high maturity organic-rich lacustrine shales (Upper Cretaceous Qingshankou Formation, Northern Songliao Basin, NE China): Implications for hydrocarbon generation and horizontal compression. *Marine and Petroleum Geology*, 158, 106544.

Trebus, K., Tarantola, A., Fabre, C., Caumon, M.-C., Cauzid, J., Motto-Ros, V., Lecomte, A., Peiffert, C., Voudouris, P., & Mavrogenatos, C., 2022. Trace Element Distribution in Zoned Kyanite of Thassos Island (Greece) Using Combined Spectroscopic Analyses. *Applied Spectroscopy*, 76(9), 1051-1067.

Ueno, K., & Charoentirat, T., 2011. Carboniferous and Permian. In M. F. Ridd, A. J. Barber, & M. J. Crow (Eds.), *The Geology of Thailand* (pp. 0). Geological Society of London.

